Hazirbaba & Omarow, *Cogent Engineering* (2019), 6: 1573788
https://doi.org/10.1080/23311916.2019.1573788

cogent engineering

CIVIL & ENVIRONMENTAL ENGINEERING | RESEARCH ARTICLE

Strain-based assessment of liquefaction and seismic settlement of saturated sand

Kenan Hazirbaba[1]* and Maksat Omarow[2]

Received: 09 August 2018
Accepted: 21 January 2019
First Published: 23 January 2019

*Corresponding author: Kenan Hazirbaba, Department of Civil and Infrastructure Engineering, American University of Ras Al Khaimah, UAE
E-mail: kenan.hazirbaba@aurak.ac.ae

Reviewing editor:
Sanjay Kumar Shukla, School of Engineering, Edith Cowan University, Australia

Additional information is available at the end of the article

Abstract: This study presents results from an extensive experimental research on saturated clean sand deposits subjected to seismic loading. A total of 29 freshly reconstituted soil samples were tested under laboratory conditions. Strain-controlled, undrained, cyclic triaxial tests were conducted to evaluate the excess pore water pressure and associated settlement response of soil to seismic loading. The level of induced cyclic shear strain varied between 0.01% and 0.5%. The generation of excess pore water pressure was measured under various consolidation stresses ranging from 100 kPa to 400 kPa. Additionally, the settlement due to the dissipation of the excess pore pressure was measured and analyzed for each level of consolidation stress. The findings from the experimental work were used for liquefaction and seismic assessment of an actual soil deposit. A scenario earthquake of magnitude *Mw* = 7.2 with peak ground acceleration (*PGA*) of 0.42 g was considered. Induced shear strains at various depths of the soil deposit were determined using software ProShake. It was found that relatively shallower depths were less prone to liquefaction with insignificant cyclic settlement.

Subjects: Civil, Environmental and Geotechnical Engineering; Foundations and Piling; Georisk & Hazards

Keywords: liquefaction of sand; cyclic settlement; cyclic strain-controlled testing; excess pore pressure generation; volumetric strain

1. Introduction

Seismic loading of saturated sand deposits leads to the development of excess pore water pressure within the soil. Increase in pore pressure, when high enough, can cause substantial loss of strength in the soil, which in turn leads to transformation of stable soil structure into an unstable liquid-like form. This phenomenon is known as liquefaction of the soil. Liquefaction of

ABOUT THE AUTHORS

Kenan Hazirbaba is an Associate Professor of Civil Engineering at the American University of Ras Al Khaimah. He received his Ph.D. from the University of Texas at Austin. As a registered professional geotechnical engineer, he worked on numerous large-scale infrastructure projects. His research interests include stabilization of marginal soils, liquefaction of shallow and deep deposits under seismic loading, and numerical studies and modeling of transport facilities and substructures.

Maksat Omarow is a former graduate student of University of Alaska.

PUBLIC INTEREST STATEMENT

Earthquakes are the major cause of failures for various structures and infrastructures. This is mainly because of the dynamic loading induced in the ground with the shaking. The supporting soil of structures and infrastructure loses its bearing capacity and turns into a liquid-like form which leads to catastrophic collapses. This study investigates the response of the supporting ground to seismic shaking and evaluates the potential of failure of the ground that can pose tremendous public hazard.

saturated soil deposits is a major cause of failure for various infrastructures as well as superstructures during earthquakes. If the developed excess pore water pressure is below the limit to cause liquefaction failure, there is still a damage potential associated with the dissipation of the pressure in the form of excessive settlement. Therefore, saturated sand deposits subjected to dynamic loading has the potential to fail because of: (i) liquefaction and (ii) excessive settlement.

To evaluate the liquefaction potential, several approaches by different researchers have been proposed (e.g. Dobry, Ladd, Yokel, Chung, & Powell, 1982; Ishihara, 1977; Iwasaki, Arakawa, & Tokida, 1984; Law, Cao, & He, 1990; Lees, Ballagh, Orense, & van Ballegooy, 2015; Maurer, Green, Cubrinovski, & Bradley, 2014; Robertson & Campanella, 1985; Seed & Idriss, 1971). The common methods in practice can be grouped under two major categories: (1) stress-based and (2) strain-based approaches. Earthquake loading and the soil liquefaction resistance are characterized in terms of cyclic stresses in the stress-based approach, and in terms of induced cyclic strains in the strain-based approach.

The stress-based procedure (Seed & Idriss, 1971) uses an approximation for the cyclic shear stress to be developed due to earthquake loading. At a depth of interest, this is done as follows:

$$\tau_{cyc} = 0.65 \frac{a_{\max}}{g} \sigma_v r_d \tag{1}$$

where a_{max} is the peak recorded acceleration at the ground surface, g is the gravitational acceleration, σ_v is the total overburden stress at the depth of consideration, and r_d is a stress reduction factor, which is used to account for the variation of shear stress with depth. The assessment of liquefaction is based on the comparison between the estimated value of cyclic shear stress, τ_{cyc}, and the cyclic shear resistance of the soil, $\tau_{cyc,L}$, (i.e, shear stress required to cause liquefaction in a given number of loading cycles). The cyclic shear resistance can be obtained from laboratory or in-situ tests. Liquefaction is predicted at the site if the equivalent shear stresses induced by the earthquake are larger than the cyclic shear resistance *($\tau_{cyc}/\tau_{cyc,L} > 1$).*

The strain-based approach (Dobry et al., 1982) requires conversion of irregular earthquake cyclic strains into uniform strain cycles. The amplitude of the uniform cyclic strain is predicted using the following expression:

$$\gamma_{cyc} = 0.65 \frac{a_{\max}}{g} \frac{\sigma_v r_d}{G(\gamma_{cyc})} \tag{2}$$

where $G(\gamma_{cyc})$ is the shear modulus of the soil at γ_{cyc}. Estimation of $G(\gamma_{cyc})$ should be performed iteratively from measured Gmax profile and appropriate modulus reduction curves (e.g. Darendeli & Stokoe, 2001; Sun, Golesorkhi, & Seed, 1988). In the field, shear modulus at small strains, Gmax, can directly be measured by geophysical techniques (Yang, Dutta, Xu, Hazirbaba, & Marx, 2011; Cox & Hazirbaba, 2012). In strain-based procedure, the liquefaction potential is determined by the level of excess pore water pressure corresponding to the induced cyclic shear strain, γ_{cyc}. Labortaory or field tests may be used to quantify the excess pore water pressure. For excess pore water pressure ratio (r_u, where $r_u = \Delta u/\sigma'$; Δu = excess pore pressure and σ' = initial effective confining pressure) value of 0.9 or greater, liquefaction is expected.

As discussed above, the key parameter in determining both the liquefaction potential and cyclic loading settlement is the excess pore water pressure. Induced shear strain is considered to be a more directly related parameter to the excess pore water pressure buildup of saturated sands during undrained cyclic loading than shear stress (Hazirbaba & Omarow, 2015, 2018). However, the challenge in the strain-based procedure is in determining the cyclic shear strain accurately. In this study, a systematic experimental program was designed to evaluate the response of a medium dense clean sand at various cyclic shear strains and consolidation stresses. The findings from this research are directly applied to a case study where an actual soil deposit is subjected to a scenario

seismic event. The details of the experimental program and the implication of the results through a case study are presented in the following sections.

2. Material and methodology

2.1. Material

Ottawa sand (C-109) was tested in this study. Ottawa sand is a commercially produced, washed, and sieved clean sand. The grain size distribution curve of the Ottawa sand is shown in Figure 1. The index property tests performed on the soil were in accordance with ASTM standards. The results are summarized in Table 1, and agree well with the previously reported studies on Ottawa sand (e.g. Carraro, Bandini, & Salgado, 2003).

2.2. Testing system

The testing equipment used in this research is a custom-made triaxial equipment. The system is equipped with signal conditioning, servo amplifier, computer interface, and data acquisition units. A dedicated software enables the system to be controlled by the computer. Servo valves are the controlling means for the hydraulically actuated axial loader as well as the pressure system. A photo of the equipment is shown in Figure 2. The triaxial cell is capable of accommodating 100 mm (diameter) by 200 mm (height) samples. Up to 32 transducers can be installed and controlled with the signal conditioning unit. Sensor capacities and sensitivities are summarized in Table 2.

2.3. Sample preparation

In this study, the moist undercompaction (Ladd, 1978) method was adopted for reconstituting the sand specimens. Dry soil was mixed with distilled, de-aired water to obtain saturation of about 50%. The mixture was prepared in an airtight container in order to uniformly distribute the moisture and prevent any loss of water due to evaporation. A rubber membrane was stretched tight to the inner wall of a split type mold with vacuum, which was then seated on the base pedestal of the triaxial apparatus, as shown in Figure 3. Moist soil was transported into the mold using a spoon. The desired layer height was achieved by using a manual tamper. After compaction, the tamper was removed and the top surface of the layer was slightly roughened in order to obtain a good contact between layers. Total of 10 layers were compacted following the same procedure. The final layer was compacted to a slightly higher height to allow some sitting for the top cap. A light twist was applied while seating the top cap in order to maintain full contact between the cap and the specimen. After connecting the drainage lines, about 20 kPa vacuum was applied and the mold was dismantled. The vacuum was applied through a burette with water. This allowed checking for any air leakage into the specimen. O-rings at the top and bottom of the specimen were tightened further around the membrane with the help of hose clamps. The dimensions of the specimen were measured and recorded. Then, the cell was assembled and filled with tap water.

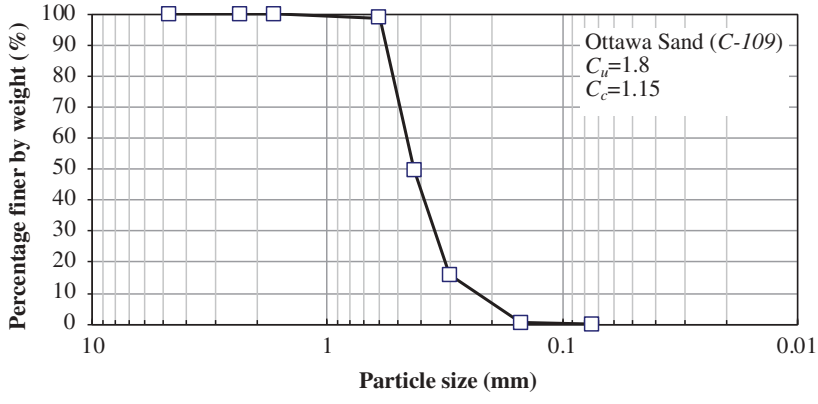

Figure 1. Grain size distribution of Ottawa sand (C-109).

Table 1. Index properties of clean Ottawa sand

	Index Properties of Ottawa Sand (C-109)
Specific Gravity	2.66
Maximum Void Ratio	0.78
Minimum Void Ratio	0.48
D_{10} (mm)	0.25
D_{30} (mm)	0.36
D_{60} (mm)	0.45
C_u	1.8
C_c	1.15
USCS Soil Classification	SP

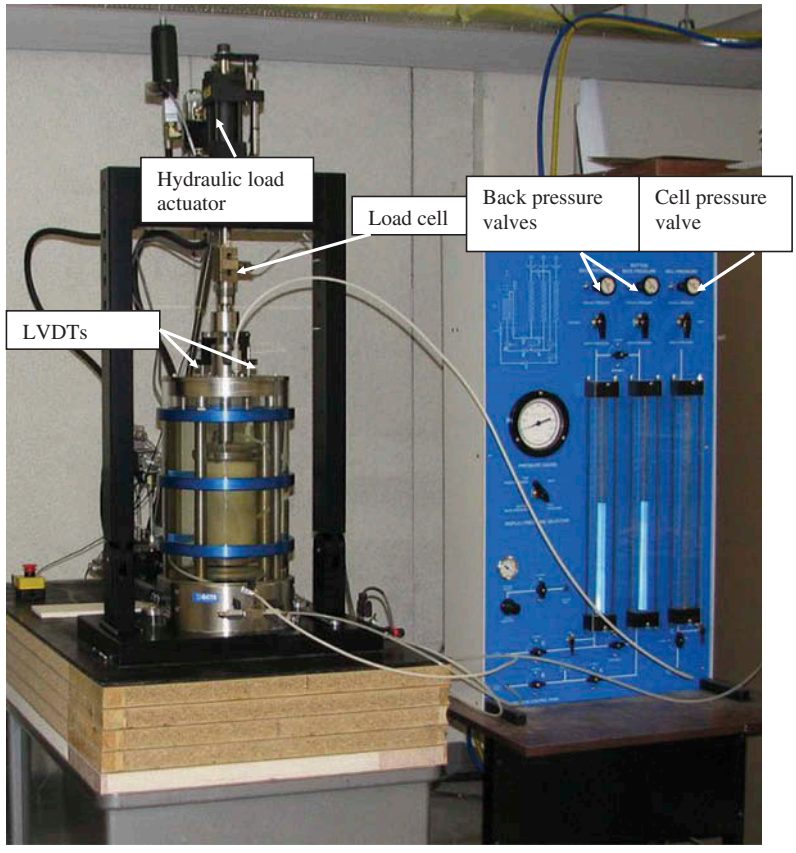

Figure 2. A photo of the cyclic triaxial testing equipment employed in this research.

Table 2. Sensor information in the triaxial equipment

Measurement	Sensor	Capacity or Range	Sensitivity
Axial Displacement (External)	Big Axial LVDT	±25.4 mm	±0.0254 mm
Axial Displacement 1	Miniature Axial LVDT	±2.54 mm	±0.0016 mm
Axial Displacement 2	Miniature Axial LVDT	±2.54 mm	±0.0016 mm
Vertical Load	Load Cell	2000 lb (8895 N)	±0. 3 lb (1.3 N)
Cell Pressure	Pressure Transducer	1000 kPa	±2.5 kPa
Back Pressure	Pressure Transducer	1000 kPa	±2.5 kPa

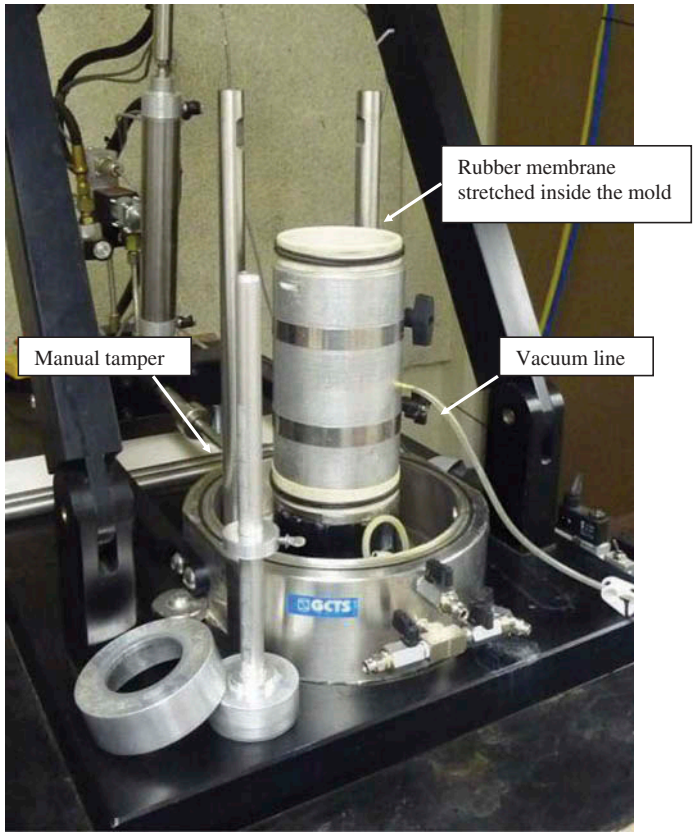

Figure 3. The mold and the manual tamper used in specimen preparation.

A cell pressure of 10 kPa was applied while releasing the vacuum. It is important not to exceed a net effective stress of 30 kPa on the sample at this stage. Next, the sample was flushed with carbon dioxide (CO_2). This is done to speed up the saturation process. Because CO_2 is much more soluble in water than air, the back-pressure saturation is achieved faster (Hazirbaba & Omarow, 2015). Following the percolation with CO_2, the sample is flushed with de-aired water. Then, back-pressure was applied while keeping the same initial net effective stress on the specimen. Full saturation was assumed to have been achieved for B-values of 0.96 or higher.

Following backpressure saturation, the sample was consolidated to the desired nominal effective stress. The sample was allowed to consolidate until no further volume change occurred, which took about 60 minutes. This was considered to be adequate due to the relatively high permeability of the sand.

2.4. Cyclic loading

The sample dimensions at the end of consolidation were used to determine the necessary axial deformation to induce the desired cyclic strain, γ. The peak to peak axial strain was calculated for the loading cycles using the consolidated height of the specimen. The cyclic shear strain can be calculated by elasticity theory, as:

$$\gamma = \varepsilon_v(1+\nu) \tag{3}$$

where γ is shear strain, ε_v is applied double amplitude axial strain, and ν is Poisson's ratio (=0.5 for fully saturated soils). The sample was subjected to sinusoidal loading at a frequency of 0.2 Hz. This loading frequency was selected for more accurate pore pressure measurements as larger frequencies were found to disrupt the pore pressure equilibration.

After 50 loading cycles or liquefaction (i.e. $r_u = 1.0$), the test was terminated and cyclic settlement (reconsolidation) measurements were conducted with the help of the volume change transducer and set-up. Dissipation of the developed excess pore pressure and associated cyclic settlement took about 30 minutes or less to complete.

Results from a typical strain-controlled, undrained, cyclic triaxial test are illustrated in Figure 4. A clean sand specimen is subjected to 0.3% cyclic shear strain as shown in Figure 4(a). The change in shear stress and excess pore water pressure with respect to the number of loading cycles is shown in Figure. 4(b,c), respectively. Figure 4(d) shows shear stress versus shear strain indicating degradation of stiffness, primarily due to the increase in the excess pore pressures.

3. Experimental results and discussion

A total of 29 tests were conducted on reconstituted medium dense (Dr = 50%) sand samples. Each test was conducted on a freshly prepared sand sample. The tests performed are listed in Table 3. The tests are grouped according to the applied consolidation stress (i.e. 100 kPa, 300 kPa, and 400 kPa).

Figure 5 illustrates the excess pore pressure buildup in terms of pore pressure ratio versus cyclic shear strain after 10 loading cycles (N = 10) for specimens tested under 100 kPa effective confining pressure. The number of loading cycles N = 10 was selected as a representative of Mw = 7.0 earthquake (Dobry et al., 1982; Seed & Idriss, 1971). The results are compared with those presented by Dobry (1985) for various sands, specimen preparation techniques, relative densities, and initial effective confining stresses. There is a reasonable agreement between the results from this study and the upper bound of Dobry (1985). It should be noted that Ottawa sand was not included among the sands investigated by Dobry. The results in Figure 5 shows that no significant excess pore pressure develops when the induced shear strains are less than about 0.01%, suggesting a threshold shear strain for Ottawa sand to be 0.01%, which agrees with Dobry's results for clean sands.

Hazirbaba (2005) introduced the rate of excess pore pressure per logarithmic cycle as a parameter characterizing pore pressure generation. The graphical illustration of the concept is given in Figure 6. Rates of pore pressure generation were calculated and evaluated in terms of effective confining pressures, as presented in Figures 7 and 8. Pore pressure generation rate is defined as the ratio of the difference in excess pore pressure ratios, Δr_u, to the difference in number of loading cycles in logarithmic scale, $\log(N_i/N_{i-1})$.

The rate curves illustrate how rapidly the excess pore pressures develop in the samples. In Figures 7 and 8, pore pressure rates of specimens subjected to lower (0.06%) and higher (0.3%) shear strains are compared for different consolidation stresses. The data show that the pore pressure rate is mainly influenced by the (i) level of shear strain, (ii) number of loading cycles, and (iii) consolidation stress.

The development of excess pore water pressure with respect to the applied shear strain comprises a set of curves when considered for different loading cycles. These curves, called pore pressure generation curves, illustrate the generation of pore pressures by each loading cycle. Pore pressure generation curves from the tests conducted in this study are shown in Figures 9–11. They show that the excess pore water pressure is a function of the applied shear strain, γ, and the number of loading cycles, N. The generated pore pressure increases with increasing induced shear strain. It can also be seen that excess pore pressures gradually increase with increasing number of loading cycles.

At a given level of induced shear strain, the potential of excess pore pressure generation is a function of the number of loading cycles. More specifically, the first and last cycles of loading may be used to evaluate the potential of pore pressure generation. The difference between the

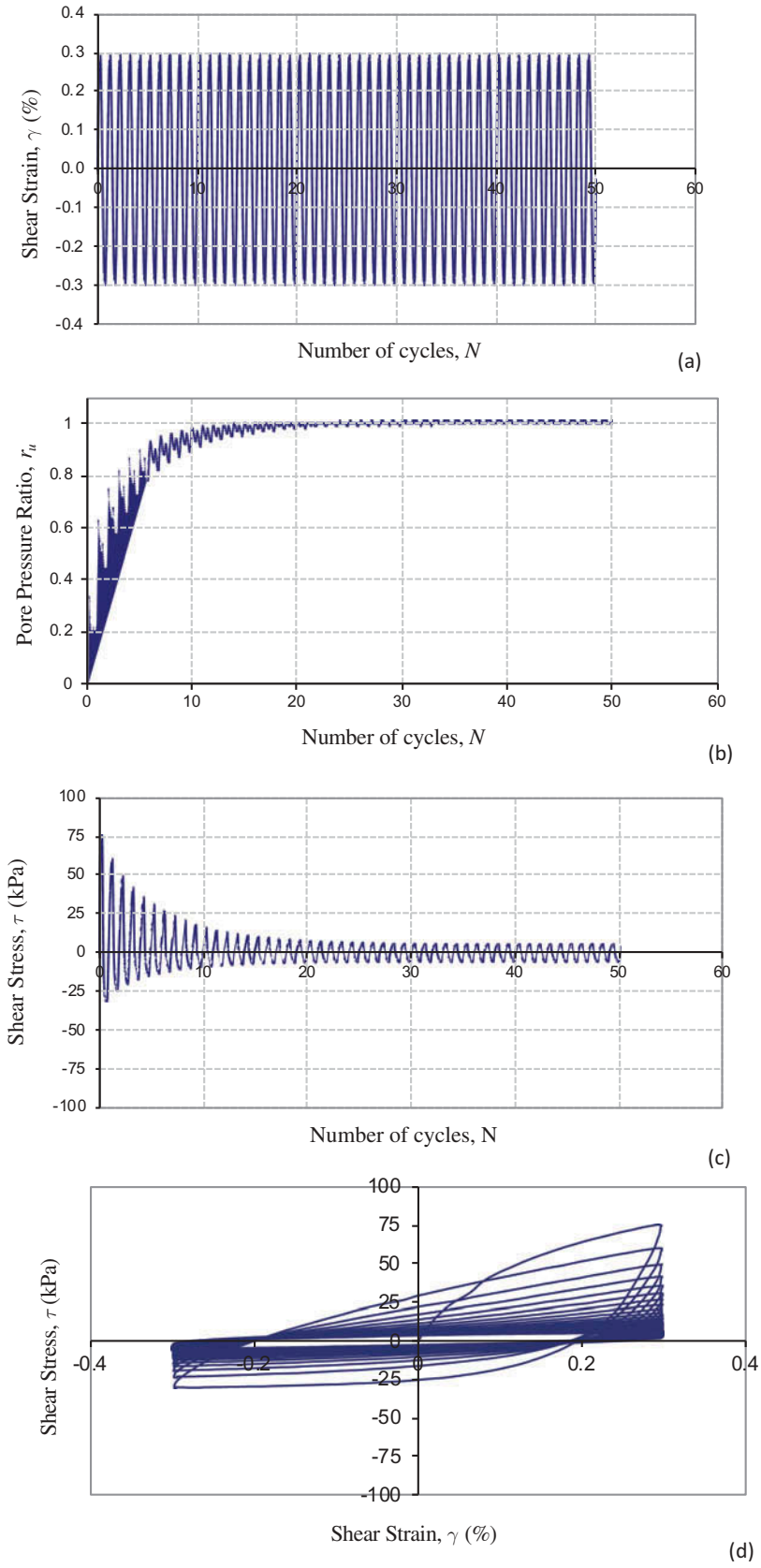

Figure 4. Typical results of a strain-controlled test.

Table 3. List of tests performed

Test No.	γ (%)	B	σ' (kPa)	Post Test ΔV (%)
1	0.001	0.97	100	0
2	0.003	0.97	100	0
3	0.005	0.97	100	0
4	0.007	0.97	100	0
5	0.010	0.97	100	0
6	0.030	0.97	100	0.0287
7	0.060	0.96	100	0.1598
8	0.100	0.99	100	0.3454
9	0.200	0.96	100	0.6982
10	0.300	0.97	100	0.9633
11	0.500	0.96	100	1.2052
12	0.001	0.96	300	0
13	0.005	0.96	300	0
14	0.007	0.96	300	0
15	0.010	0.96	300	0.0307
16	0.020	0.97	300	0.0230
17	0.030	0.98	300	0.0305
18	0.050	0.98	300	0.1554
19	0.060	0.96	300	0.1844
20	0.100	0.98	300	0.4586
21	0.200	0.96	300	0.7941
22	0.300	0.96	300	1.0801
23	0.500	0.96	300	1.5298
24	0.010	0.97	400	0
25	0.030	0.96	400	0.0460
26	0.060	0.98	400	0.0918
27	0.100	0.98	400	0.2752
28	0.200	0.96	400	0.6485
29	0.300	0.96	400	1.0383

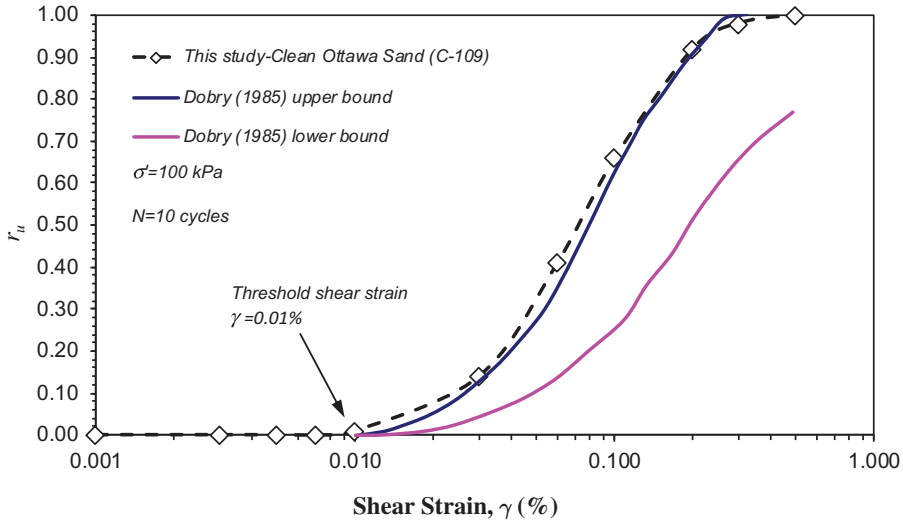

Figure 5. Pore pressure ratio versus cyclic shear strain after 10 cycles of loading.

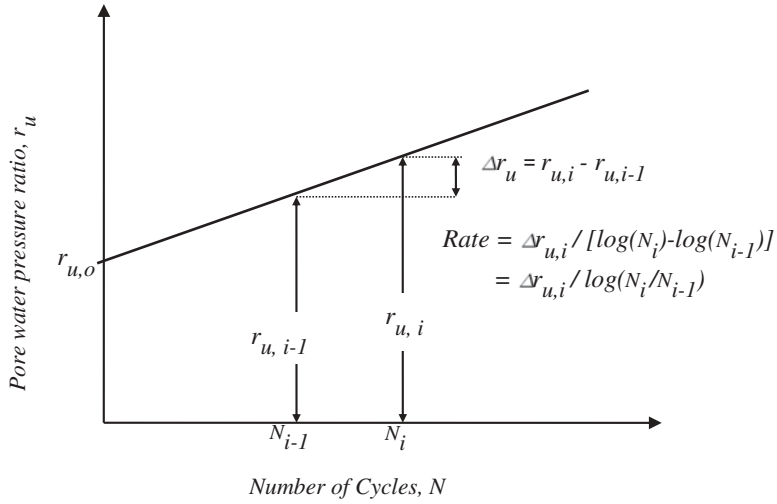

Figure 6. Conceptual representation of excess pore water pressure generation per logarithmic cycle (by Hazirbaba, 2005).

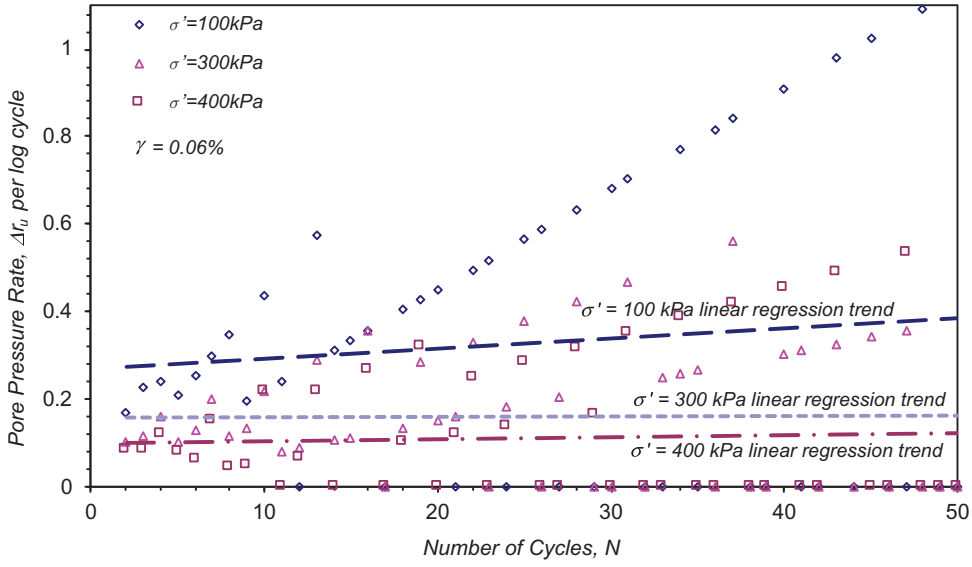

Figure 7. Pore pressure rate versus number of loading cycles for γc = 0.06%.

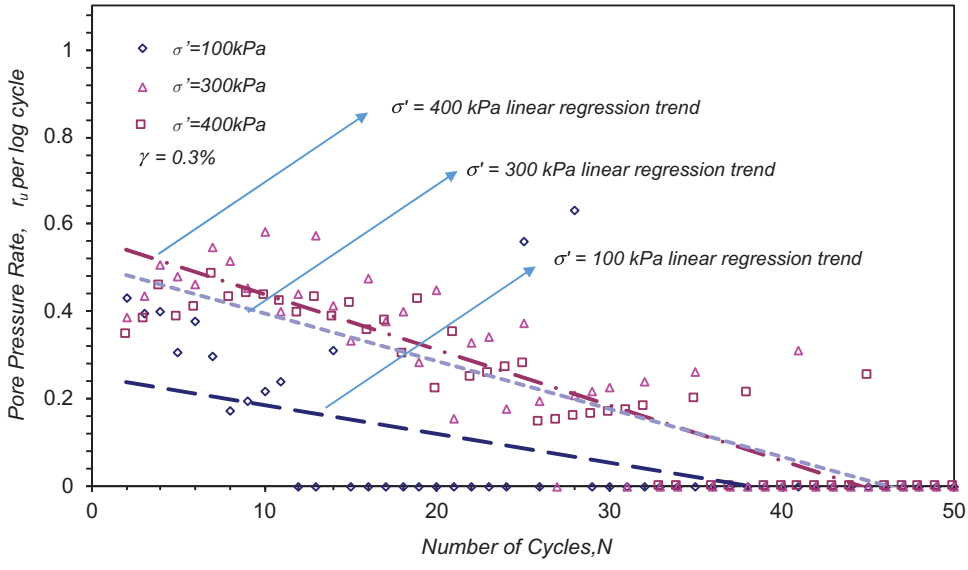

Figure 8. Pore pressure rate versus number of loading cycles for γc = 0.3%.

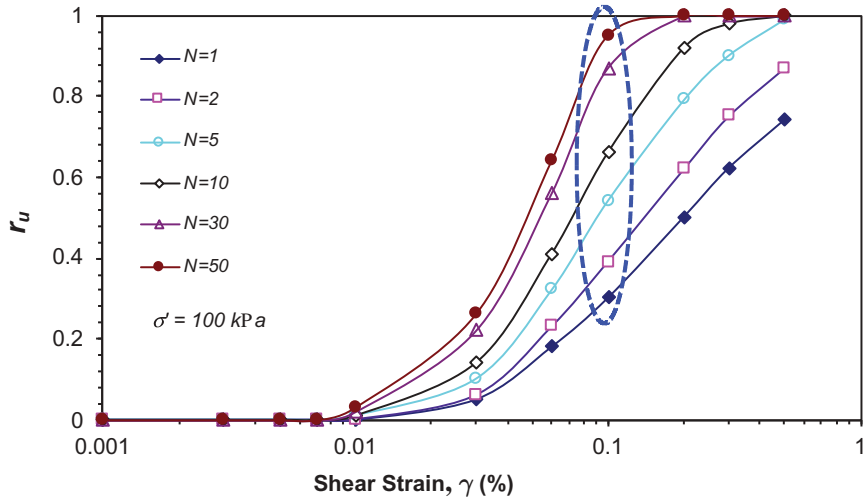

Figure 9. Excess pore water pressure generation as a function of cyclic shear strain and loading cycles under σ_c' = 100 kPa.

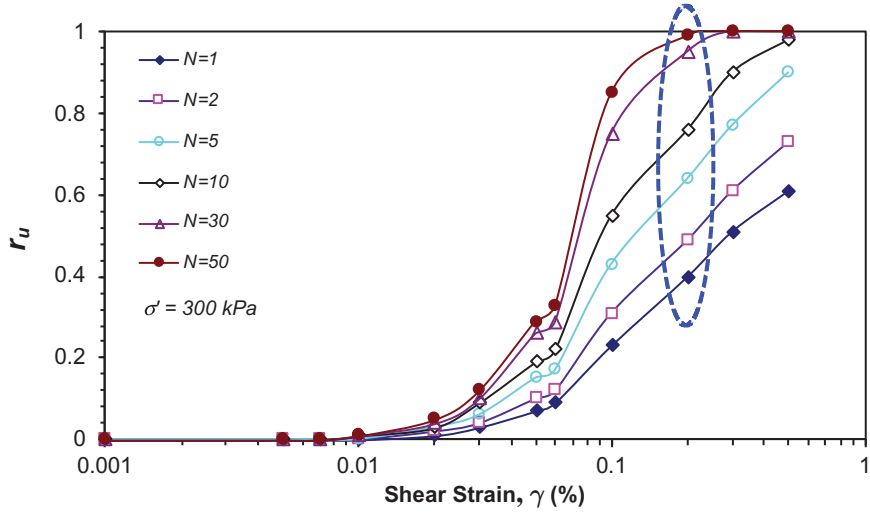

Figure 10. Excess pore water pressure generation as a function of cyclic shear strain and loading cycles under σ_c' = 300 kPa.

pore pressure ratios at these loading cycles (i.e. first and last) can quantify the potential; the larger the difference, the greater the potential. At relatively small levels of induced shear strain (γ ~ 0.01%) the difference is negligible. This is confirming the existence of the threshold shear strain level below which neither pore pressure develops nor settlement occurs. As the shear strain level increases beyond the threshold value of 0.01%, the difference becomes more pronounced. For the specimen consolidated to 100 kPa effective stress (Figure 9), the largest difference is observed at shear strain of 0.1% indicating a significant influence of the number of loading cycles on excess pore pressure development. However, once close to liquefaction (i.e. excess pore pressure ratio of 1.0), the curve flattens out and the difference in pore pressure between loading cycles decreases. Therefore, specimens consolidated to 100 kPa effective stress are mostly influenced by the number of loading cycles in the middle range shear strains (γ ~ 0.1%) as shown with the dashed ellipse. For specimens with higher consolidation stresses of 300 kPa and 400 kPa, the influence region (dashed ellipse) is shifted towards higher shear strains (γ) of 0.2% and 0.3%, respectively, as shown in Figures 10 and 11. Thus, the results presented in Figures 9–11 imply that the generation of pore pressure requires a greater level of induced shear strain with increasing consolidation stress in the range of 100 kPa to 300 kPa.

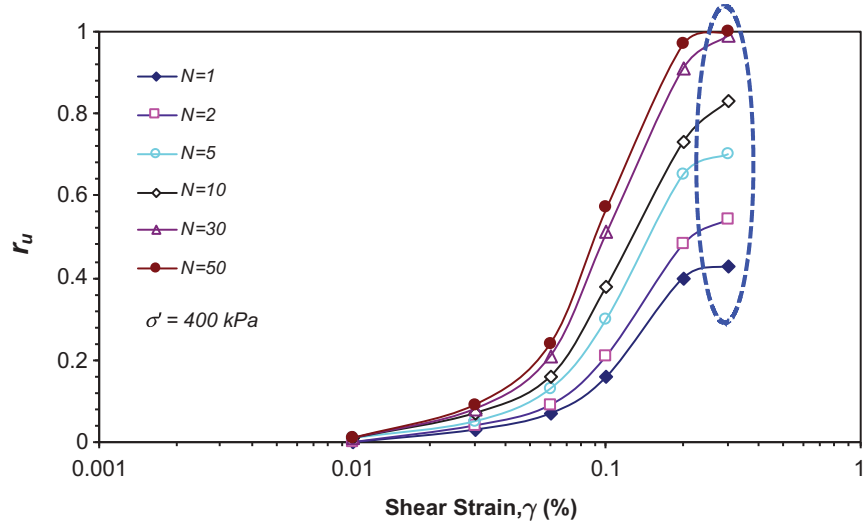

Figure 11. Excess pore water pressure generation as a function of cyclic shear strain and loading cycles under σ_c' = 400 kPa.

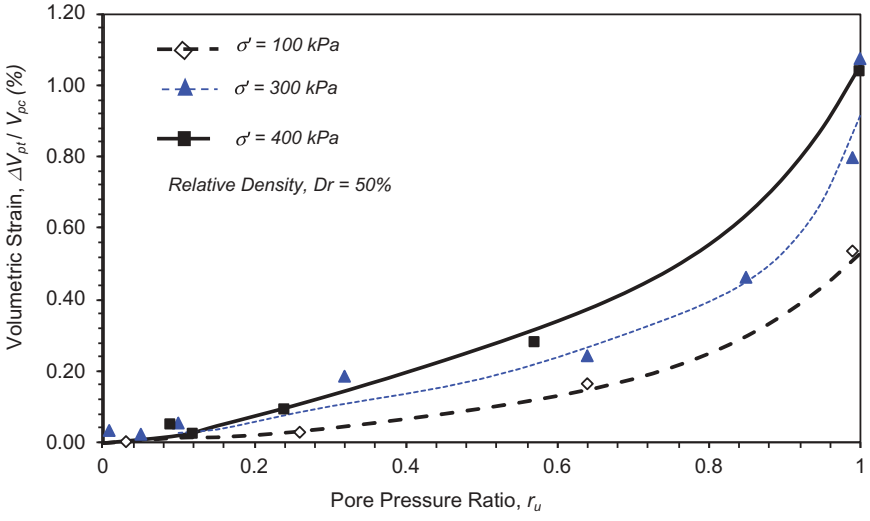

Figure 12. Measured volumetric strains versus pore pressure ratio under different consolidation stress.

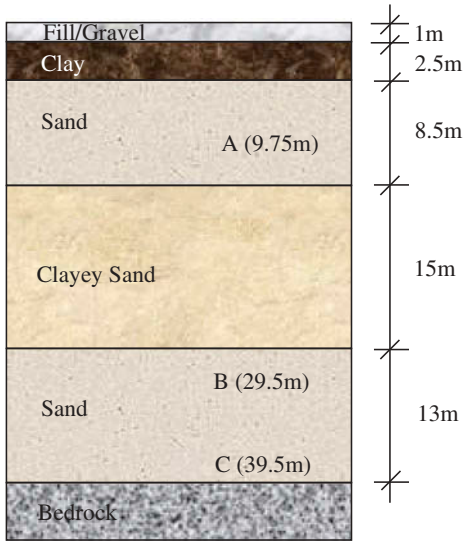

Figure 13. Soil profile evaluated for liquefaction potential and cyclic settlement.

Table 4. Properties of the soil profile shown in Figure 13

Layer	Depth (m)	Soil	Unit weight (kN/m^3)	G_{max} (MPa)	V_s (m/s)
1	0–1	Gravel	22	291	360
2	1–3.5	Clay	18	120	255
3	3.5–12	Sand	19.8	168	290
4	12–27	Clayey Sand	20	182	299
5	27–40	Sand	20.4	325	395
6	40-infinite	Rock	25	3371	1150

The volumetric strain is calculated as the ratio between post-loading volume change and the post-consolidation (pre-loading) volume of the specimen, $\varepsilon_v = \Delta V_{pt}/V_{pc}$. Volumetric strains were analyzed against generated pore water pressure as shown in Figure 12. It can be seen that for the same value of generated excess pore pressure, the volumetric strain increased with increasing effective confining pressure. However, the influence is not very strong and becomes more pronounced at higher excess pressures. Lee and Albaisa (1974) reported similar results stating that the influence of the effective confining pressure was only significant for pore pressures higher than 0.6.

4. Implication of the results through a case study

The findings of the current research were used to evaluate the liquefaction potential and cyclic settlement of the soil profile shown in Figure 13. The soil profile consists of considerable amount of medium dense (*Dr* = 50%) sand deposit, confined by impermeable clay and bedrock layers. The water table is 0.5 m from the ground surface. The properties of the soil are summarized in Table 4. It should be noted that these properties were compiled as representative values based on the soil type. The soil deposit was subjected to a scenario earthquake of magnitude *Mw* = 7.2 with peak ground acceleration (*PGA*) of 0.42 g. Figure 14 shows the synthetic ground motion characteristics.

Corresponding depths to the effective consolidation stresses considered previously (σ' = 100 kPa, 300 kPa and 400 kPa) are points *A, B,* and *C*, as shown in Figure 13. The induced shear strains at these points were determined using the software "ProShake". The results of the analyses are provided in Figure 15. The induced maximum shear strain due to the seismic event at points *A, B,* and *C* are γ_{max} = 0.047%, 0.98%, and 1.48%, respectively. Equivalent uniform, cyclic shear strains are calculated by multiplying the maximum shear strains by a factor of 0.65 (65% of the maximum shear strain) as per Equation (2). Therefore, uniform cyclic shear strains at points *A, B,* and *C* are γ = 0.03%, 0.64%, and

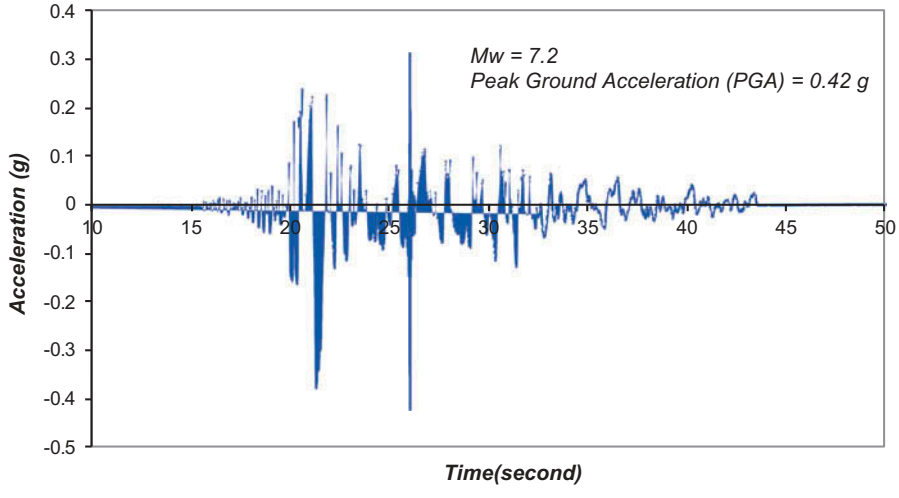

Figure 14. Ground motion characteristics of the scenario earthquake.

Figure 15. Induced shear strains in the ground due to the scenario earthquake.

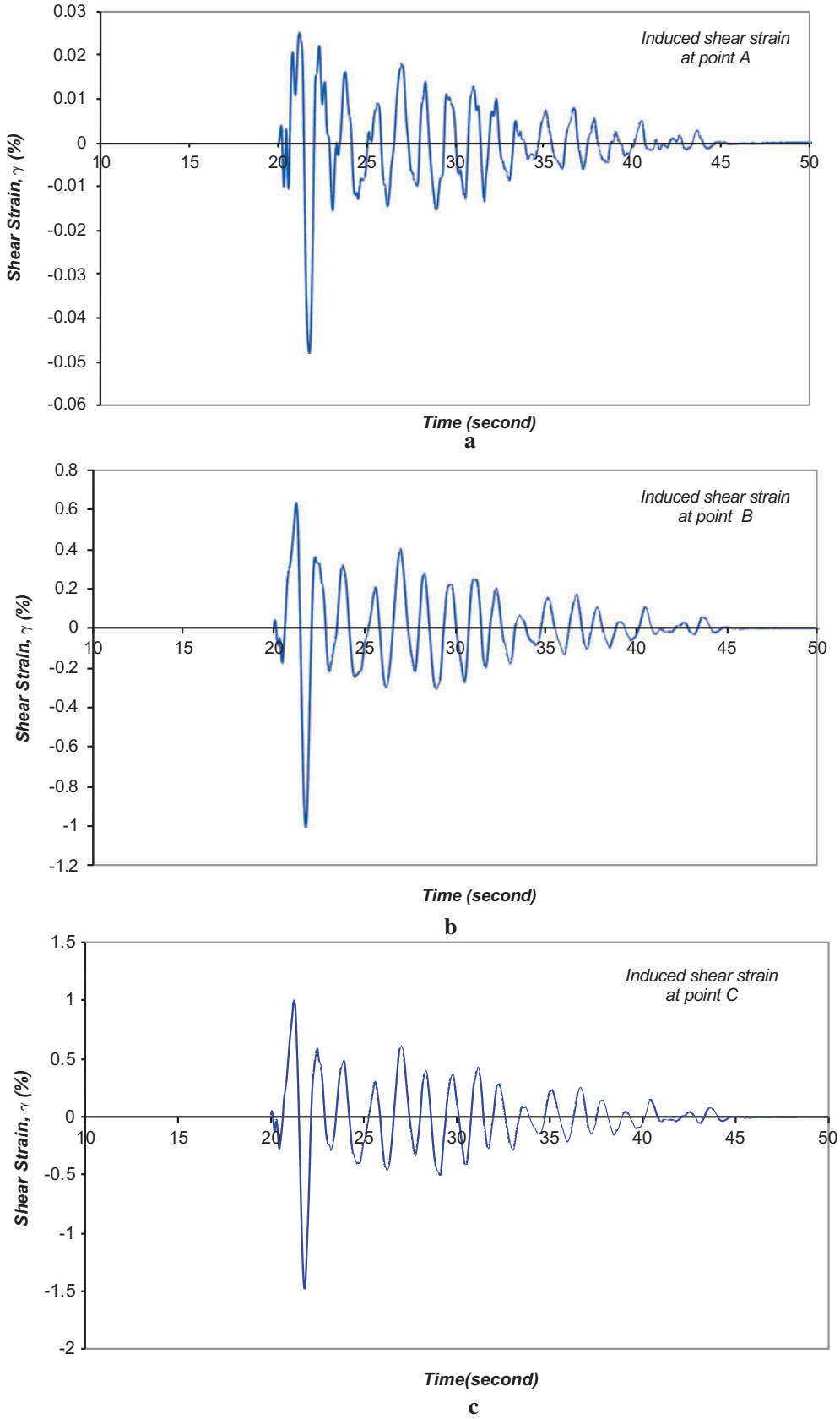

Table 5. Reconsolidation settlements at points A, B, and C due to the considered earthquake.

Point	Depth (m)	Max. Shear Strain, γ_{max} (%)	Cyclic Shear Strain, γ (%)	Residual Pore Pressure Ratio, r_u	Volumetric Strain, ε_v (%)
A	9.75	0.047	0.03	0.14	0.04
B	29.5	0.98	0.64	>0.98	0.9
C	39.5	1.48	0.96	>0.8	0.6

0.96%, respectively. The number of uniform loading cycles corresponding to earthquake magnitude Mw = 7.2 is N = 10 (Dobry, 1985). Thus, the excess pore pressures are estimated as $r_{u.A}$ = 0.14; $r_{u.B}$ > 0.98; and $r_{u.C}$ > 0.8 from Figures 9–11, respectively. It is important to note that the maximum cyclic shear strain for the samples tested under 300 kPa and 400 kPa consolidation stress in the laboratory were 0.5% and 0.3%, respectively. The excess pore pressure ratio at these levels of induced shear strain was found to be at a near-liquefaction state (r_u > 0.8). Therefore, points *B* and *C* are likely to experience liquefaction.

Settlement due to the dissipation of the generated pore pressures can be estimated using Figure 12. The settlement values in the form of volumetric strains at points *A, B,* and *C* are obtained approximately as ε_v = 0.04%, 0.9% and 0.6%, respectively, and listed in Table 5.

5. Summary and conclusion

A series of strain-controlled, undrained, cyclic triaxial tests were performed on samples of medium dense sand. The excess pore water pressure and the settlement due to the dissipation of this pressure were evaluated, and applied to a case study. The following conclusions were drawn from this study:

(1) Results from tests performed on samples consolidated to different effective stresses show that generated excess pore pressures decrease with increasing consolidation stress. The influence in the mid-range shear strains (γ = 0.03–0.3%) was found to be significant; more than 200% reduction in pore pressure was observed for samples consolidated to 400 kPa in comparison to those consolidated to 100 kPa.

(2) The pore pressure was found to increase with increasing number of loading cycles and induced shear strain. At a given level of induced shear strain, the potential to develop excess pore pressure was evaluated by analyzing the difference between the first and last loading cycles. The larger the difference, the greater the potential of pore pressure generation.

(3) The number of loading cycles was found to be an essential parameter in determining (i) pore pressure generation potential of a specimen and (ii) rate of pore pressure development.

(4) Evaluation of volumetric strain as a function of generated pore pressure showed that samples consolidated to higher effective consolidation stresses experience larger volumetric strain.

(5) Assessment of liquefaction potential of an actual soil deposit was illustrated through a case study. The deeper layers of soil in the deposit with 300 kPa and 400 kPa consolidation stresses were found to be more susceptible to liquefaction under the scenario seismic event. The shallower location was found to be far less susceptible to liquefaction.

(6) The analysis of settlement, in the form of volumetric strain, indicated much greater potential of failure at deeper layers of soil under the scenario event.

Acknowledgements

Funding for this research was provided by U.S. DOT, Research and Innovative Technology Administration through Alaska University Transportation Center, and State of Alaska Department of Transportation & Public Facilities under the Grant No. G3238–33650. This funding is gratefully acknowledged. Any opinions, findings and conclusions or recommendations expressed in this material are those of the author and do not necessarily reflect the views of the sponsors for this research.

Funding

This work was supported by the U.S. DOT, Research and Innovative Technology Administration through Alaska

University Transportation Center, and State of Alaska Department of Transportation & Public Facilities [Grant number: G3238-33650].

Author details
Kenan Hazirbaba[1]
E-mail: kenan.hazirbaba@aurak.ac.ae
Maksat Omarow[2]
E-mail: momarow@alaska.edu
[1] Department of Civil and Infrastructure Engineering, American University of Ras Al Khaimah, Ras Al Khaimah, UAE.
[2] University of Alaska, USA.

Citation information
Cite this article as: Strain-based assessment of liquefaction and seismic settlement of saturated sand, Kenan Hazirbaba & Maksat Omarow, *Cogent Engineering* (2019), 6: 1573788.

References

Carraro, J. A. H., Bandini, P., & Salgado, R. (2003). Liquefaction resistance of clean and nonplastic silty sands based on cone penetration resistance. *Journal of Geotechnical and Geoenvironmental Engineering, ASCE*, *129*(11), 965–976.

Cox, B., Wood, C., & Hazirbaba, K. (2012). Frozen and unfrozen shear wave velocity seismic site classification of fairbanks. *Alaska. Journal of Cold Regions Engineering, ASCE*, *26*(3), 118–145.

Darendeli, M. B., & Stokoe, K. H. (2001). *Development of a new family of normalized modulus reduction and material damping curves* (Geotechnical Engineering Report GD01-1). The University of Texas at Austin.

Dobry, R. (1985). *Liquefaction of soils during earthquake* (Report No. CETS-EE-001). Washington, DC: National Research Council (NRC), Committee on Earthquake Engineering

Dobry, R., Ladd, R. S., Yokel, F. Y., Chung, R. M., & Powell, D. (1982). Prediction of pore water pressure buildup and liquefaction of sands during earthquakes by the cyclic strain method. *National Bureau of Standards Building Science Series*, *138*, 150.

Hazirbaba, K. (2005). *Pore pressure generation characteristics of sands and silty sands a strain approach* (Ph.D. Dissertation). University of Texas at Austin, p. 232.

Hazirbaba, K., & Omarow, M. (2015). Post-cyclic loading settlement of saturated clean sand. *Soil Dynamics and Earthquake Engineering*, *77*, 337–347.

Hazirbaba, K., & Omarow, M. (2018). Excess pore pressure generation and post-cyclic loading settlement of geofiber-reinforced sand. *Gradevinar*, *70*(2018) 1, 11–18.

Ishihara, K. (1977). Simple method of analysis for liquefaction of sand deposits during earthquakes. *Soils and Foundations*, *17*(3), 1–17.

Iwasaki, T., Arakawa, T., & Tokida, K. (1984). Simplified procedures for assesing soil liquefaction during earthquakes. *Soil Dynamics and Earthquake Engineering*, *3*(1), 49–58.

Ladd, R. S. (1978). Preparing test specimens using undercompcation. *Geotechnical Testing Journal, GTJODJ*, *1*(1), 16–23.

Law, K. T., Cao, Y. L., & He, G. N. (1990). Energy approach for assessing seismic liquefaction potential. *Canadian Geotechnical Journal*, *27*(3), 320–329.

Lee, K. L., & Albaisa, A. (1974). Earthquake induced settlements in saturated sands. *Journal of the Geotechnical Engineering Division, ASCE*, *100*(GT4), 387–406.

Lees, J. J., Ballagh, R. H., Orense, R. P., & van Ballegooy, S. (2015). CPT-based analysis of liquefaction and re-liquefaction following the Canterbury earthquake sequence. *Soil Dynamics and Earthquake Engineering*, *79*, 304–314.

Maurer, B. W., Green, R. A., Cubrinovski, M., & Bradley, B. A. (2014). Evaluation of the liquefaction potential index for assessing liquefaction potential in Christchurch, New Zealand. *Journal of Geotechnical and Geoenvironmental Engineering*, *140*, 04014032.

Robertson, P. K., & Campanella, R. G. (1985). Liquefaction potential of sands using the CPT. *Journal of Geotechnical Engineering Division, ASCE*, *111*(3), 38–40.

Seed, H. B., & Idriss, I. M. (1971). Simplified procedure for evaluating soil liquefaction potential. *Journal of the Soil Mechanics and Foundations Division, ASCE*, *97* (SM9), 1249–1273.

Sun, J. I., Golesorkhi, R., & Seed, H. B. (1988). *Dynamic moduli and damping ratios for cohesive soils* (Report No. EERC-88/15). Berkley: Earthquake Engineering Research Center, University of California.

Yang, Z., Dutta, U., Xu, G., Hazirbaba, K., & Marx, E. (2011). Numerical analysis of permafrost effects on the seismic site response. *Soil Dynamics and Earthquake Engineering*, *Elsevier*, *31*(3), 282-290.

***Cogent Engineering* (ISSN: 2331-1916) is published by Cogent OA, part of Taylor & Francis Group.**